Chemical Science

ROYAL SOCIETY OF CHEMISTRY

EDGE ARTICLE

View Article Online
View Journal | View Issue



Cite this: *Chem. Sci.*, 2020, **11**, 12547

All publication charges for this article have been paid for by the Royal Society of Chemistry



# Controlled hierarchical self-assembly of networked coordination nanocapsules *via* the use of molecular chaperones†

Xiangquan Hu,[a] Sisi Feng,*[b] Jialei Du,*[c] Li Shao,[a] Jinxin Lang,[d] Chen Zhang,[e] Steven P. Kelley,[a] Jian Lin,[f] Scott J. Dalgarno,[g] David A. Atwood[h] and Jerry L. Atwood*[a]

Supramolecular chaperones play an important role in directing the assembly of multiple protein subunits and redox-active metal ions into precise, complex and functional quaternary structures. Here we report that hydroxyl tailed *C*-alkylpyrogallol[4]arene ligands and redox-active $Mn^{II}$ ions, with the assistance of proline chaperone molecules, can assemble into two-dimensional (2D) and/or three-dimensional (3D) networked $Mn^{II}_{24}L_6$ nanocapsules. Dimensionality is controlled by coordination between the exterior of nanocapsule subunits, and endohedral functionalization within the 2D system is achieved *via* chaperone guest encapsulation. The tailoring of surface properties of nanocapsules *via* coordination chemistry is also shown as an effective method for the fine-tuning magnetic properties, and electrochemical and spectroscopic studies support that the $Mn^{II}_{24}L_6$ nanocapsule is an effective homogeneous water-oxidation electrocatalyst, operating at pH 6.07 with an exceptionally low overpotential of 368 mV.

Received 9th September 2020
Accepted 16th October 2020

DOI: 10.1039/d0sc05002d

rsc.li/chemical-science

## Introduction

Hierarchical self-assembly *via* metal coordination is a ubiquitous process for constructing sophisticated supramolecular structures in nature.[1] As an example of its use in biological systems, metal coordination or bridging plays a crucial role in folding and assembling multiple protein subunits into precise, complex and functional quaternary structures (such as viral metalloproteins).[2,3] Metallosupramolecular assemblies such as metal–organic nanocapsules (MONCs) and/or nanocages are potentially useful models for such complex biological processes,[4,5] and are also promising with regard to energy storage,[6–10] molecular encapsulation,[11–15] catalytic,[16–18] and biomedical applications.[19,20] To date, synthetic chemists have been able to isolate discrete cages consisting of more than 100 precisely designed units through metal coordination.[21] A long-standing challenge, however, is the rational combination of simple components to form hierarchical superstructures with a similar level of assembly complexity as proteins.[22,23] Another challenge that has seldom been addressed in the literature is redox-controlled metal-directed assembly. Albeit at a higher level of complexity, living organisms are able to rapidly select the oxidation state of metal ions such as Cu, Mn and Fe, with regard to protein subunit folding and assembly of quaternary structure, often with the aid of supramolecular chaperones.[24–26] These metallochaperones are typically employed to capture, protect and insert the highly active metal ions into the specific coordination sites before elements of the quaternary structure have formed through subunit self-assembly.[26] The powerful self-assembly approach utilised by biological systems may thus provide access to new hierarchical superstructures (HSSs) with unique properties.

Our group (and others) have used *C*-alkyl-pyrogallol[4]arenes ($PgC_n$, where $n$ is the number of carbon atoms in the pendant alkyl chains), bowl-shaped polydentate macrocycles, to synthesise MONCs *via* metal insertion.[13,27,28] This approach gives rise to large, discrete cages which typically have one of two highly conserved structures: a dimeric cage composed of 2 $PgC_n$s seamed/bridged by 8 metal ions, or a hexameric cuboctahedral analog comprising 6 $PgC_n$s and 24 metal ions (the latter of which form 6 triangular faces). These MONCs are readily

[a]*Department of Chemistry, University of Missouri-Columbia, 601 S College Ave, Columbia, MO 65211, USA. E-mail: atwood@missouri.edu*

[b]*Key Laboratory of Chemical Biology and Molecular Engineering of Ministry of Education, Institute of Molecular Science, Shanxi University, Taiyuan 030006, P. R. China. E-mail: ssfeng@sxu.edu.cn*

[c]*Institute for Advanced Interdisciplinary Research, University of Jinan, Jinan 250022, P. R. China. E-mail: ifc_dujl@ujn.edu.cn*

[d]*School of Chemistry, Xi'an Jiaotong University, Xi'an 710049, P. R. China*

[e]*Department of Chemical and Biomolecular Engineering, North Carolina Sate University, Raleigh, North Carolina 27695, USA*

[f]*Department of Mechanical and Aerospace Engineering, University of Missouri-Columbia, 601 S College Ave, Columbia, MO 65211, USA*

[g]*Institute of Chemical Sciences, Heriot-Watt University, Riccarton, Edinburgh EH14 4AS, UK*

[h]*Department of Chemistry, University of Kentucky, Lexington, KY 40506, USA*

† Electronic supplementary information (ESI) available. CCDC 1981690 and 1981691. For ESI and crystallographic data in CIF or other electronic format see DOI: 10.1039/d0sc05002d

accessible *via* ambient or solvothermal syntheses using redox stable metal ions such as $Zn^{II}$, $Ni^{II}$, $Ga^{III}$.[28–30] Variations in structure are also possible, for instance by replacing some pyrogallol rings with resorcinol in the $PgC_n$ framework, giving mixed macrocycles that cause 'defects' in the perfect MONC structure.[29] Despite the fact that these two general supramolecular architectures accommodate metals of different size and charge, the controlled assembly of redox-active transition metals has proven difficult. For instance, it has been shown that the reaction of $Fe^{II}$ or $Mn^{II}$ ions with $PgC_n$s rapidly yielded MONCs with metal ions in mixed oxidation states.[31,32] Indeed, the assembly of mixed-valence MONCs, such as $Mn^{II}/Mn^{III}$, should be more kinetically favored than solely $Mn^{II}$-based analogs since $Mn^{II}$ is more thermodynamically stable and kinetically labile than $Mn^{III}$ for coordination.[26] We only recently achieved the assembly of $Co^{II}$ hexameric MONCs by using a route inspired by zinc-finger proteins (ZNFs).[33] In that case the $Zn^{II}$ ion was used to direct assembly of hexameric MONCs that were spontaneously transmetallated with $Co^{II}$ ions to afford the target assembly. Such results indicate that new MONCs with redox-active functionality may (as can be the case with biological systems) require additional templates or chaperones to control their assembly into the correct state.

In this context, we are encouraged to challenge the synthesis of HSSs constructed from *C*-propan-3-ol-pyrogallol[4]arene ($PgC_3OH$) and coordination-inert but redox-active $Mn^{II}$ ions; the hydroxyl group on $PgC_3OH$ can link MONCs to obtain HSSs.[30] This may not only help to develop a better understanding of the redox-based self-assembly of metalloproteins, but also the construction of HSSs with emergent properties, such as magnetism and catalysis, based on the oxidation state distribution of the metal ions.[34–36] Several reaction conditions and methodologies have been investigated to this end, yet all failed to deliver the selective assembly of any anticipated HSSs (see ESI† for details). We hypothesised that *in situ* redox reactions may prevent the formation of such highly intricate structures.

Herein, we present a design strategy for the construction of such otherwise unobtainable HSSs that uses a reaction system consisting of $PgC_3OH$, $Mn^{II}$ ions, and proline. The use of proline was inspired by the $Mn^{II}$ coordination sphere in manganese-based proteins, which may effectively capture and stabilise the free metal ion, as well as modulating its weak coordination ability with regard to metal insertion.[26,37,38] We propose a system in which $PgC_3OH$ is assembled into hexameric hydrogen-bonded nanocapsules (MONCs), whilst proline molecules act as the molecular chaperones to capture, protect and insert the $Mn^{II}$ ions into the framework (Scheme 1). Once formed, the thermodynamically and kinetically very stable MONCs serve as subunits (secondary structures) and organise into more complex HSSs through the formation of intermolecular metal–hydroxyl coordination bonds. Using this approach, we obtained 2D and 3D HSSs consisting of $Mn^{II}$-seamed MONC subunits (**1**, $[Mn_{24}(PgC_3OH)_6(H_2O)_{44}]$ and **2**, $[Mn_{24}(PgC_3OH)_6(H_2O)_{44}(CH_3CN)_2]$), structurally controlled by subtle changes in reaction conditions.

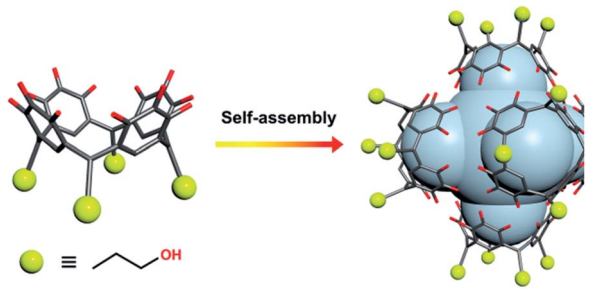


Scheme 1 Pre-assembly strategy of $Mn^{II}$-seamed MONC subunits used in this study. Color codes: carbon, grey; oxygen, red; $Mn^{II}$, purple.

## Results and discussions

Compound **1** has been studied and characterised by scanning electron microscopy images (Fig. S1†), single-crystal X-ray diffraction (SC-XRD, Fig. S2†), FT-IR (Fig. S3†), elemental analysis (EA), MALDI-TOF MS (Fig. S4†), thermogravimetric analysis (TGA, Fig. S5†) and differential scanning calorimetry (DSC, Fig. S6†), details of which can be found in the ESI.† Compound **1** crystallises in the monoclinic space group $P2_1/n$. The crystal structure of **1** shows a 2D framework constructed from infinite MONCs subunits, with each MONC being assembled from 30 components: six $PgC_3OH$ molecules and 24 metal ions (Fig. 1). The overall geometry of the MONC subunit corresponds to that of a truncated octahedron, which is similar to the previously reported hexameric MONCs.[28] Each hexagonal face of the MONC is capped by one $[Mn_3O_3]$ trimetallic cluster with Mn–O distances in the range of 2.03–2.11 Å, Mn–O–Mn angles in the range of 133.17–137.50°, and O–Mn–O angles in the range of 99.34–105.66°. All $Mn^{II}$ ions adopt an octahedral ligand field, where the equatorial positions are coordinated with oxygen atoms from the upper-rim of $PgC_3OH$ units. Bond-valence sum (BVS) analysis, coupled with examination of bonding energy reveals that all Mn ions are in the +2 oxidation state (Table S1 and Fig. S7†). Interestingly, each MONC encapsulates two proline chaperone ligands that coordinate in

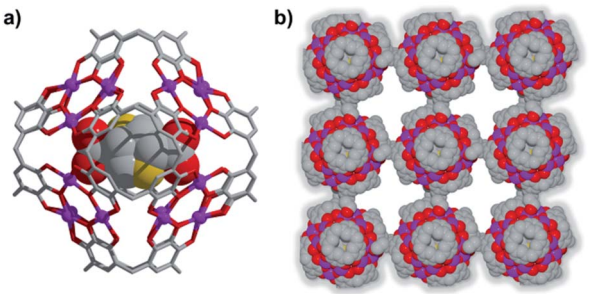


Fig. 1 (a) Side and (b) extend views of the single crystal X-ray structure of **1**. Inspection shows 2D HSSs composed of $Mn^{II}$-MONC subunits, each of which encapsulates two proline chaperone molecules *via* metal coordination. Color codes: manganese (purple), carbon (grey), oxygen (red), nitrogen (yellow). Hydrogen atoms, axial water ligands and hydroxyl tail alkyl chains not involved in metal–ligand coordination to adjacent MONC subunits were removed for clarity.

a bridging mode between two $Mn^{II}$ ions (metal–carboxyl distances in the range of 2.24–2.27 Å). This suggests that the proline molecules perform the critical function of a molecular chaperone, capturing, protecting and inserting $Mn^{II}$ ions into MONCs *via* ligand exchange during the assembly process. The extended view of **1** shows that each MONC is connected to four adjacent symmetry equivalents *via* double manganese–hydroxyl coordination (M–O distances: 2.26–2.35 Å). One MONC provides a hydroxyl tail and a metal coordination site for another, and the other axial positions are occupied by water molecules.

Introduction of a greater amount of water to similar reaction conditions as those used in the synthesis of **1** changed both the internal and external properties of the $Mn^{II}$-seamed MONCs, resulting in the formation of a 3D HSSs which crystallises in an orthorhombic system (structure solution in space group *Pccn*, **2**, Fig. 2, Table S2 and Fig. S8–S10†). On the internal surface, all axial positions at the metal centres are occupied by water molecules, whilst inspection of the exterior reveals that each MONC subunit is linked to eight symmetry equivalents *via* single manganese–hydroxyl coordination bonds (two crystallographic M–O distances: 2.276 and 2.279 Å, respectively), the result being assembly into a cubic tertiary structure (Fig. 2b). This supramolecular nanocube is assembled from 216 $Mn^{II}$ ions and 54 $PgC_3OH$ macrocyclic ligands and has an edge of 4.5 nm. Within the nanocube there are two types of MONC subunits with different orientation in the solid lattice, highlighted by the disparate colours in Fig. 2. This structural motif is similar to the unit cell of CsCl (Fig. 2c), and the extended view exhibits a hierarchical CsCl-like superstructure (Fig. 2d).

Magnetic susceptibility data for **1** and **2** were recorded in the temperature range of 2.0–300 K in an applied magnetic field of 1000 Oe. The $\chi_m$, $\chi_m T$ *vs.* $T$ plots for the complexes are shown in Fig. 3, where $\chi_m$ is the molar magnetic susceptibility. For supramolecular assemblies **1** and **2**, the values of $\chi_m T$ at 300 K are 81.8 and 92.2 $cm^3\ mol^{-1}$ K, respectively, but lower than that of expected for the sum of the Curie constants for 24 non-interacting $Mn^{II}$ ($s = 5/2$) ions, with $g = 2.00$ (105.0 $cm^3\ mol^{-1}$ K). Upon cooling, $\chi_m T$ first gradually decreases to a value of 76.1 $cm^3$ K $mol^{-1}$ at 100 K, and then decreases more rapidly on further cooling to 27.3 $cm^3$ K $mol^{-1}$ at 2.0 K for **1**, however, $\chi_m T$ decreases to the minimum value of 29.4 $cm^3\ mol^{-1}$ K at 2.0 K for **2**, indicating antiferromagnetic coupling within the $Mn^{II}$ ions. Above 50 K, the temperature dependence of $\chi_m{}^{-1}$ obeys the Curie–Weiss law with $C = 90.91$ $cm^3$ K $mol^{-1}$ and $\theta = -12.8$ K above 2.0 K for **1** and $C = 102.88$ $cm^3\ mol^{-1}$ K and $\theta = -41.8$ K for **2** (see Fig. 3, inset). The negative $\theta$ values confirm the antiferromagnetic coupling within the $Mn^{II}$ ions and the antiferromagnetic coupling in **2** is stronger than that in **1**. Furthermore, the shapes of the $M/H$ plots are quite like that of the antiferromagnet, in which the $M$ values increase rapidly at low fields, with no obvious saturation observed up to 70 kOe (Fig. S11 and 12†).

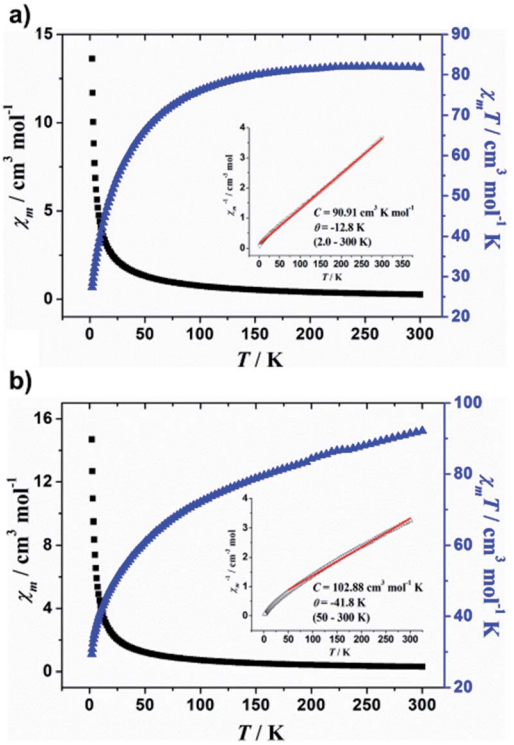


Fig. 3 Temperature dependence of $\chi_m$, $\chi_m T$, and $\chi_m{}^{-1}$ (inset) collected in applied field of 1000 Oe for (a) **1** and (b) **2**. Red solid line represents best fits.

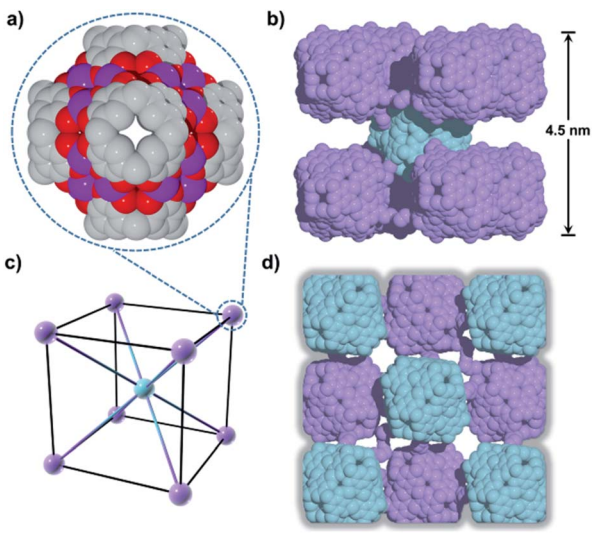


Fig. 2 (a) $Mn^{II}$-seamed MONC subunits (secondary structure). (b) Supramolecular nanocubes (tertiary structure). (c) CsCl unit cell and (d) the 3D hierarchical CsCl-like superstructure (quaternary structure). Hydrogen atoms, axial ligands and hydroxyl tail alkyl chains not involved in metal–ligand coordination to adjacent MONC subunits were removed for clarity.

Water oxidation (WO, $2H_2O \rightarrow O_2 + 4H^+ + 4e^-$) is regarded as a key half-reaction for solar fuel production.[39] The rational design and synthesis of cheap, efficient and stable water-oxidising catalysts are significant challenges in science and technology.[40] In nature, the oxygen-evolving complex (OEC, a $CaMn_4O_5$ cluster) in photosystem II (PS II) can efficiently oxidize water.[41] It has been shown that the $Mn^{IV}$–O–$Mn^{III}$–$H_2O$ motif plays a crucial role in the activity of the OEC and its

mimics.[42] Inspired by the OEC, several Mn clusters have been used as structural mimics. In particular, the presence of high oxidation state +3 and +4 Mn ions and four water binding sites have been applied for electrocatalytic oxidation of water, examples such as $Mn_{12}O_{12}(OAc)_{16-x}L_x(H_2O)_4$ (L = acetate, benzoate, benzenesulfonate, diphenylphosphonate, and dichloroacetate).[43–45] However, the catalytic activity of these biomimetic Mn-based clusters for water oxidation was shown to be hindered by either high overpotentials (ranging from 640–820 mV) or low structural stability.[40] Kinetically and thermodynamically very stable Mn clusters assembled with exclusively $Mn^{II}$ ions may solve one of such problem even though a series of mononuclear manganese complexes $[(Py_2NR_2)Mn^{II}(H_2O)_2]^{2+}$ (R = H, Me, *t*Bu) were reported to be active in electrocatalytic water oxidation with an relatively high overpotential of approximately 800 mV (FTO working electrode).[34] However, to the best of our knowledge it remains unknown whether polynuclear $Mn^{II}$ clusters are capable of being highly active with respect to water oxidation.

This long-standing question has been examined with **1** and **2** using electrochemical techniques. Crystals of **1** and **2** were dissolved in 0.1 M aqueous acetate buffer at pH 6.07 *via* sonochemistry, the pH at which the OEC within PSII shows optimal catalytic performance.[46] The resulting solutions of **1** and **2** were subjected to UV-Vis spectroscopy and showed two broad absorption bands at around $\lambda_{max}$ = 262 and 315 nm for **1** and $\lambda_{max}$ = 260 and 312 nm for **2**, which can be assigned to the π–π* transition and ligand-to-metal charge transfer transition, respectively (Fig. S13†). The redox peaks associated with manganese of **1** and **2** in aqueous acetate buffer have been detected *via* cyclic voltammetry (Fig. 4a, b and S14†). These corresponded to the oxidation of $Mn^{2+}$ to $Mn^{4+}$ ($E$ = 0.87 V) and the reduction of $Mn^{4+}$ to $Mn^{3+}$ ($E$ = 0.83 V), $Mn^{4+}$ to $Mn^{2+}$ ($E$ = 0.55 V), and $Mn^{3+}$ to $Mn^{2+}$ ($E$ = 0.26 V).[47] The solution stability of the coordination structures was investigated using dynamic light scattering (DLS) techniques. It was shown that sonication of these solutions resulted in the formation of species in the size range of 2–3 nm, corresponding to the molecular hydrodynamic diameter of discrete MONCs (Fig. S15†),[13] and implying that HSSs converted into discrete MONCs; we envisage that some metal-coordinated hydroxyl groups of $PgC_3OH$ moieties on axial positions may be displaced by water molecules. Interestingly, upon evaporation of an aqueous acetate buffer solution of **1** and **2**, spherical, micron-scale metallosuperstructures were observed by SEM (Fig. 4c, d and S16†). FT-IR and small angle X-ray scattering studies further supported that they were composed of many MONC subunits (Fig. S17 and 18†). We propose that the hierarchical metal–organic micron spheriods (MOMSs) may be stabilized by a large number of van der Waals interactions between neighboring alkyl chains and hydrophilic regions of the discrete MONCs.

Furthermore, cyclic voltammograms (CVs) clearly indicated that water oxidation can be catalyzed by both **1** and **2** (Fig. 5).[43,47] Water oxidation occurs at an exceptionally low overpotential of only 368 mV. This is higher than that of the current state-of-art Ru-bda complex (bda = 2,2′-bipyridine-6,6′-dicarboxylate, 180 mV at pH 7), illustrating that there is still room for further improvements.[48] Continuous CV scan experiments and bulk electrolysis of **1** and **2** demonstrated that these electrocatalysts have high catalytic activity and stability toward water oxidation (Fig. S19 and 20†). UV-Vis and DLS measurements taken after electrolysis of **1** and **2** showed that the waves and particle size are retained (Fig. S21 and 22†). Moreover, the MOMSs re-formed and could be detected upon evaporation of the catalyst solution in subsequent SEM studies (Fig. S23†). Collectively, these measurements suggest that the MONC subunit is a homogeneous water oxidation electrocatalyst. This result may thus provide a new strategy for the design and synthesis of cheap, efficient and stable water-oxidizing catalysts since it first suggests that soluble $Mn^{II}$ clusters may be used to effectively facilitate the oxidation of water, despite the enormous efforts made to mimic the $CaMn_4O_5$ cluster to date. We further envision that improvements of catalyst stability and activity may be possible. This may be achieved through (for example) attaching appropriate axial ligands to the constituent metal ions, or functionalizing alkyl chains on the MONC surface. In addition, other soluble metal-seamed dimeric or hexameric MONCs, such as those formed with $Fe^{II}$, $Co^{II}$ and $Cu^{II}$ ions, are also promising with regard to electrocatalytic water oxidation.[36]

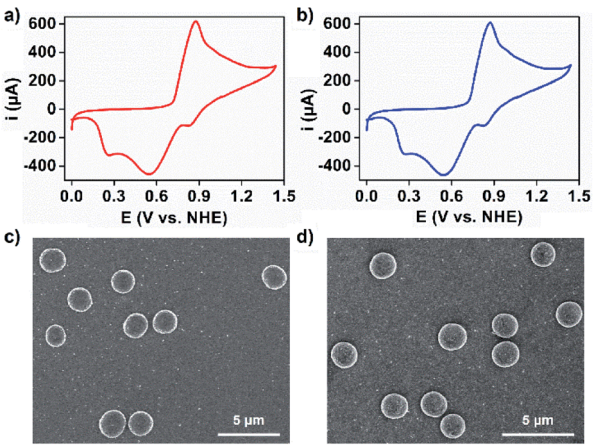


Fig. 4 Cyclic voltammograms (CVs) of (a) **1** and (b) **2** (0.5 mM) in 0.1 M acetate buffer at pH 6.07 using an FTO ($S$ = 1 $cm^2$) working electrode. Scan rate is 50 mV $s^{-1}$. SEM images of hierarchical micron spheroids formed from an aqueous acetate buffer of (c) **1** and (d) **2**.

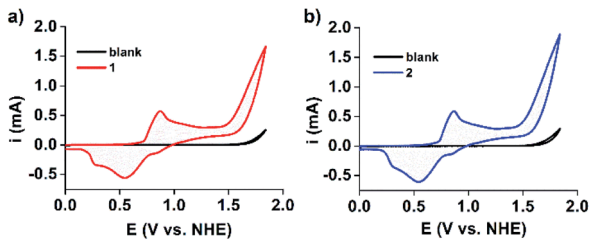


Fig. 5 CV scans of (a) **1** and (b) **2** (0.5 mM, 50 mV $s^{-1}$ scan rate) in 0.1 M acetate buffer at pH 6.07. For comparison, CVs of the blank buffer are also shown. FTO ($S$ = 1 $cm^2$) was used as the working electrode.

## Conclusions

In summary, we have developed a new strategy for the rational construction of HSSs using biomimetic self-assembly as the synthetic methodology. Akin to the self-assembly behaviours of protein subunits with redox-active metal ions, the assembly of these sophisticated supramolecular architectures has been accomplished by employing proline molecules as molecular chaperones to selectively insert redox-active $Mn^{II}$ ions into the coordination sites of a pre-assembled ONC skeleton, which further directs the $Mn^{II}$-seamed MONC subunits to fold and assemble into more complex HSSs across different dimensionality. This is achieved *via* control of both interior and/or exterior surface properties of the MONC subunits, through coordination and host–guest chemistries, also allowing for the fine-tuning of magnetic properties. The catalytic activity and stability of $Mn^{II}_{24}L_6$ MONCs toward homogeneous water oxidation at pH 6.07 with an exceptionally low overpotential of only 368 mV is noteworthy.

Overall, this approach represents an important advancement in supramolecular chemistry by design. Further efforts will be invested in the design and synthesis of extremely challenging and complex HSSs with other redox-active or coordinatively inert metal ions (*e.g.* $Cr^{II}/Cr^{III}$ and $Fe^{II}/Fe^{III}$), as well as inserting suitably functionalized guest molecules for potential application in the areas of molecular electronics/magnets and catalysis, all of which may be modulated by appropriate molecular chaperones. Finally, this strategy may be widely exploited in the rational design and synthesis of other metal–organic systems, such as metal–organic cages (MOCs), polyhedra (MOPs) or artificial metalloproteins, the properties and/or functions of which can be subsequently tailored accordingly.

## Conflicts of interest

The authors declare no conflict of interest.

## Acknowledgements

We thank University of Missouri for financial and research facility support of this work. We thank the U.S. National Science Foundation for support of this work (1825352). This work was also partially supported by the Natural Science Foundation of Shandong Province (ZR2018BB035, 2019GSF109013), Shanxi Province (201701D121039).

## Notes and references

1 T. Zhou, D. H. Hendrickson, Q. J. Sattentau and P. D. Kwong, *Proc. Natl. Acad. Sci. U. S. A.*, 2005, **102**, 14575–14580.
2 Y. Lu, N. Yeung, N. Sieracki and N. M. Marshall, *Nature*, 2009, **460**, 855–862.
3 E. N. Salgado, R. J. Radford and F. A. Tezcan, *Acc. Chem. Res.*, 2010, **43**, 661–672.
4 R. A. Bilbeisi, T. K. Roson and J. R. Nitschke, *Angew. Chem., Int. Ed.*, 2013, **52**, 9027–9030.
5 J. L. Atwood, L. J. Barbour, S. J. Dalgarno, M. J. Hardie, C. L. Raston and H. R. Webb, *J. Am. Chem. Soc.*, 2004, **126**, 13170–13171.
6 T. R. Cook, Y. Zheng and P. J. Stang, *Chem. Rev.*, 2013, **113**, 734–777.
7 Z. Niu, S. Feng, X. Liu, J. Ma, S. Ma and P. Cheng, *J. Am. Chem. Soc.*, 2015, **137**, 14873–14876.
8 J. J. Perry IV, J. A. Perma and M. J. Zaworotko, *Chem. Soc. Rev.*, 2009, **38**, 1400–1417.
9 T.-F. Liu, P.-Y. Chen, A. A. Yakovenko and H.-C. Zhou, *J. Am. Chem. Soc.*, 2012, **134**, 17358–17361.
10 H. Furukawa, J. Kim, N. W. Ockwig, M. O'Keeffe and O. M. Yaghi, *J. Am. Chem. Soc.*, 2008, **130**, 11650–11661.
11 D. Zhang, T. K. Roson and J. R. Nitschke, *Acc. Chem. Res.*, 2018, **51**, 2423–2436.
12 H. Kumari, C. A. Deakyne and J. L. Atwood, *Acc. Chem. Res.*, 2014, **47**, 3080–3088.
13 S. Chakraborty and G. R. Newkome, *Chem. Soc. Rev.*, 2018, **47**, 3991–4016.
14 M. Yoshizawa and L. Catti, *Acc. Chem. Res.*, 2019, **52**, 2392–2404.
15 K. Harris, D. Fujita and M. Fujita, *Chem. Commun.*, 2013, **49**, 6703–6712.
16 C. J. Brown, F. D. Toste, R. G. Bergman and K. N. Raymond, *Chem. Rev.*, 2015, **115**, 3012–3035.
17 Y. Inokuma, M. Kawano and M. Fujita, *Nat. Chem.*, 2011, **3**, 349–358.
18 Y. Yu and J. Rebek, *Acc. Chem. Res.*, 2018, **51**, 3031–3040.
19 H. Sepehrpour, X. Fu, Y. Sun and P. J. Stang, *J. Am. Chem. Soc.*, 2019, **141**, 14005–14020.
20 Y. Fang, X. Lian, Y. Huang, G. Fu, Z. Xiao, Q. Wang, B. Nan, J.-P. Pellois and H.-C. Zhou, *Small*, 2018, **14**, 1802709.
21 Q. Sun, J. Iwasa, D. Ogawa, Y. Ishido, S. Sato, T. Ozeki, Y. Sei, K. Yamaguchi and M. Fujita, *Science*, 2010, **328**, 1144–1147.
22 P. F. Damasceno, M. Engel and S. C. Glotzer, *Science*, 2012, **337**, 453–457.
23 L. Peng, N. A. Vermeulen, C. D. Malliakas, D. A. Gomez-Gualdron, A. J. Howarth, B. L. Mehdi, A. Dohnalkova, N. D. Browning, M. O'Keeffe and O. K. Farha, *Science*, 2017, **356**, 624–627.
24 L. A. Finney and T. V. O'Halloran, *Science*, 2003, **300**, 931–936.
25 A. C. Rosenzweig, *Chem. Biol.*, 2002, **9**, 673–677.
26 J. W. Whittaker, *Biochim. Biophys. Acta*, 2010, **2**, 298–307.
27 K. Su, M. Wu, D. Yuan and M. Hong, *Nat. Commun.*, 2018, **9**, 1–6.
28 S. J. Dalgarno, N. P. Power and J. L. Atwood, *Coord. Chem. Rev.*, 2008, **252**, 825–841.
29 D. A. Fowler, A. S. Rathnayake, S. Kennedy, H. Kumari, C. M. Beavers, S. J. Teat and J. L. Atwood, *J. Am. Chem. Soc.*, 2013, **135**, 12184–12187.
30 C. Zhang, R. S. Patil, C. Liu, C. L. Barnes, T. Li and J. L. Atwood, *J. Am. Chem. Soc.*, 2017, **139**, 2920–2923.
31 A. S. Rathnayake, H. W. L. Fraser, E. K. Brechin, S. J. Dalgarno, J. E. Baumeister, J. White, P. Rungthanaphatsophon, J. R. Walensky, C. L. Barnes, S. J. Teat and J. L. Atwood, *Nat. Commun.*, 2018, **9**, 1–6.

32 A. S. Rathnayake, H. W. L. Fraser, E. K. Brechin, S. J. Dalgarno, J. E. Baumeister, J. White, P. Rungthanaphatsophon, J. R. Walensky, S. P. Kelley, C. L. Barnes and J. L. Atwood, *J. Am. Chem. Soc.*, 2018, **140**, 15611–15615.
33 X. Hu, J. Chai, C. Zhang, J. Lang, S. P. Kelley, S. Feng, B. Liu, D. A. Atwood and J. L. Atwood, *J. Am. Chem. Soc.*, 2019, **141**, 9151–9154.
34 G. Karotsis, S. J. Teat, W. Wernsdorfer, S. Pilligkos, S. J. Dalgarno and E. K. Brechin, *Angew. Chem., Int. Ed.*, 2009, **48**, 8285–8288.
35 P. Dechambenoit and J. R. Long, *Chem. Soc. Rev.*, 2011, **40**, 3249–3265.
36 W.-T. Lee, S. B. Munoz, D. A. Dickie and J. M. Smith, *Angew. Chem., Int. Ed.*, 2014, **53**, 9856–9859.
37 K. J. Waldron, J. C. Rutherford, D. Ford and N. J. Robinson, *Nature*, 2009, **460**, 823–830.
38 J. R. Calhoun, F. Nastri, O. Maglio, V. Pavone, A. Lombardi and W. F. DeGrado, *J. Pept. Sci.*, 2005, **80**, 264–278.
39 K. J. Young, B. J. Brenan, R. Tagore and G. W. Brudvig, *Acc. Chem. Res.*, 2015, **48**, 567–574.
40 A. I. Nguyen, *Proc. Natl. Acad. Sci. U. S. A.*, 2019, **116**, 11630–11639.
41 S. Mukhopadhyay, S. K. Mandal, S. Bhaduri and W. H. Armstrong, *Chem. Rev.*, 2004, **104**, 3981–4026.
42 A. K. Poulsen, A. Rompel and C. J. McKenzie, *Angew. Chem., Int. Ed.*, 2005, **44**, 6916–6920.
43 Y. Mousazade, M. R. Mohammadi, P. Chernev, R. Bikas, R. Bagheri, Z. Song, T. Lis, H. Dau and M. M. Najafpour, *Catal. Sci. Technol.*, 2018, **8**, 4390–4398.
44 Y. Yan, L. S. Lee and A. A. Ruddy, *Inorg. Chem.*, 2015, **54**, 4550–4555.
45 G. Maayan, N. Gluz and G. Christou, *Nat. Catal.*, 2018, **1**, 48–54.
46 H. Schiller and H. Dau, *J. Photochem. Photobiol., B*, 2000, **55**, 138–144.
47 Y. Du, Z. Fu and L. Bi, *Dalton Trans.*, 2018, **47**, 7282–7289.
48 B. Zhang and Li. Sun, *J. Am. Chem. Soc.*, 2019, **141**, 5565–5580.